Transport and Communications Science Journal

COMPARATIVE ASSESSMENT OF HYDRATION-HEAT CHARACTERISTICS AND EARLY-AGE THERMAL CRACKING POTENTIAL OF HIGH-STRENGTH MASS CONCRETE CONTAINING FLY ASH AND SILICA FUME

Tuyet Thi Hoang, Tu Anh Do*, Viet Hai Hoang, Duc Chinh Ngo

University of Transport and Communications, 3 Cau Giay, Lang, Hanoi, Vietnam

ARTICLE INFO
TYPE: Research Article
Received: 13/10/2026
Revised: 10/11/2026
Accepted: 12/11/2026
Published online: 15/11/2026
https://doi.org/10.47869/tcsj.77.9.9

* *Corresponding author*
Email: doanhtu@utc.edu.vn (Tu Anh Do)

Abstract. This paper compares the effects of fly ash (FA) and silica fume (SF) replacement on the hydration heat characteristics and early-age thermal cracking potential of high-strength concrete in a single bridge-pier cross-section. Experimental data from two independent experimental programs comprising two mixture series (FA: 0-30%; SF: 0-15%) were evaluated using within-series control normalization. The eight mixtures were assessed for a common 2.0 m × 3.0 m section under the same seven-day thermal-mechanical analysis conditions. Maximum adiabatic temperature rise decreased by 17.6% for FA30 and 7.3% for SF15 relative to their respective controls; at 10% replacement, the reductions were 4.5% for FA and 5.2% for SF. Despite the greater heat reduction in the FA series, its maximum cracking index increased from 0.9793 (FA00) to 1.0241 (FA30), with FA30 alone exceeding the adopted stress-to-strength threshold of 1.0. In contrast, SF10 and SF15 reduced the maximum cracking index by 4.51% and 6.58%, respectively, relative to SF00; the corresponding indices were 0.8343 and 0.8162. These contrasting trends show that the benefits of reducing hydration heat cannot be assessed independently of early-age tensile strength development. For the investigated section and boundary conditions, SF at 10-15% provided the more favorable combined response, whereas increasing FA replacement reduced heat release without improving the calculated cracking index. The findings are comparative and specific to the studied series of mixtures and structural scenario.

Keywords: Hydration heat, Adiabatic temperature rise, Fly ash, Silica fume, Early-age thermal cracking

© 2026 University of Transport and Communications

1. INTRODUCTION

The thermal response of mass concrete develops from the interaction of cement hydration, heat dissipation, and restraint. Heat generated within a relatively large section cannot escape as rapidly as at its exposed faces, so the resulting temperature differences induce strains that may be restrained internally or externally. Whether these strains cause early cracking depends not only on the temperature field but also on the evolving tensile resistance, stiffness, and time-dependent deformation of the concrete [1-3]. This concern is relevant to bridge piers, pier caps, foundations and other thick structural components.

Partial replacement of Portland cement by supplementary cementitious materials (SCMs) offers one route to moderating thermal development. However, fly ash (FA) and silica fume (SF) change hydration kinetics and strength development in different ways. Their influence on peak adiabatic temperature rise cannot, by itself, establish the likelihood of thermal cracking. The question is therefore not simply which binder releases less heat, but which mixture maintains a more favorable relationship between thermally induced tensile stress and tensile capacity during the critical early-age period [4-6].

Recent experimental investigations reinforce this distinction. Work on high-strength mass concrete incorporating fly ash and slag showed the importance of selecting SCM proportions in relation to measured temperature response [7]. Temperature-stress testing of high-volume FA concrete has also been used to examine cracking resistance directly rather than inferring it from hydration heat alone [8]. Field monitoring and thermal analysis of mass-concrete structures further illustrate why section geometry and environmental exposure must be included in thermal-control assessments [9]. In parallel, calorimetric research has demonstrated the sensitivity of fly-ash hydration behavior to both replacement content and curing temperature [10].

For SF-modified high-strength concrete, a recent experimental and numerical study reported adiabatic temperature rise, early-age properties, and thermal cracking indices at replacement levels of 0-15% [11]. Its findings provide a particularly relevant reference point for the SF dataset examined here. The present article does not treat that SF-only evidence as a previously unexplored material effect. Instead, it revisits the SF response within a broader, explicitly comparative assessment that also includes FA mixtures and a consistent cross-family cracking criterion.

The FA and SF experimental programs conducted at the University of Transport and Communications supply comparable binder contents and water-to-binder ratios, but they are not a single randomized experiment: their aggregate proportions, admixture products, and initial material conditions differ [12-14]. Accordingly, absolute differences between the two control mixes cannot be attributed to FA or SF. This study addresses that limitation by reporting changes relative to each family's own control and by applying a common 2.0 m × 3.0 m pier-section thermal-stress framework. The SF-section calculations reported here were rerun for this comparison, whereas the FA results are drawn from the documented source analysis [12].

The principal research question is whether a mixture ranking based on adiabatic temperature rise remains valid when early-age tensile demand is normalized by the strength available at the same time. To answer it, the analysis distinguishes the magnitude and timing of heat release from structural temperature evolution, thermal stress, and tensile-strength development. The resulting interpretation is confined to the eight tested mixtures and the boundary conditions adopted for the reference pier.

The specific contributions of the comparative analysis are:

- A traceable integration of four SF and four FA mixtures, explicitly retaining the distinctions between the original experimental programs.
- A consistent extraction of kinetic descriptors from the available SF adiabatic histories, including characteristic times, short-interval temperature-rise rates and equivalent cumulative heat.
- A common structural basis for interpreting hydration behavior through seven-day coupled temperature-stress responses in a representative bridge-pier section.
- Within-family quantification of the heat reduction and change in maximum cracking index, thereby limiting confounding from differences between the two control mixes.
- A conditional replacement-range assessment that combines thermal and mechanical indicators without claiming an optimum beyond the mixtures and exposure conditions studied.

2. EXPERIMENTAL DATABASE AND ANALYTICAL METHODS

2.1. Mixture families and source data

Both programs used the same Portland cement (VICEM But Son PC40; Blaine fineness 375 m^2/kg; C_3S 51.74%, C_2S 24.2%, C_3A 8.16%, and C_4AF 10.35%), crushed limestone coarse aggregate with a maximum size of 12.5 mm, natural sand with a fineness modulus of 2.7, and a polycarboxylate-based high-range water reducer conforming to ASTM C494 Type G. The mixtures were proportioned according to ACI 211.4R-08 [15] with a constant binder content of 530 kg/m^3 and a water-to-binder ratio of 0.32, and the mineral admixtures replaced cement by mass. The silica fume was a commercial product conforming to ASTM C1240 (Sikacrete PP1). The fly ash was a Class F ash (ASTM C618) from the Pha Lai thermal power plant, with $SiO_2 + Al_2O_3 + Fe_2O_3 = 88.1\%$, $CaO = 1.25\%$, and a specific gravity of 2.35. The mixture proportions are listed in Table 1.

In the SF family [13], designed for a specified compressive strength of 55 MPa, the binder content was 530 kg/m^3 of total cementitious material with a water-to-binder ratio of 0.32. Cement was replaced by 0%, 5%, 10%, and 15% SF, denoted SF00, SF05, SF10, and SF15. Compressive and splitting tensile strengths were measured on 150 mm × 300 mm cylinders at 1, 2, 3, 7, and 28 days (ASTM C39 and C496; three specimens per age), together with adiabatic temperature histories, hydration parameters, and coefficients of thermal expansion (CTE) [13,14]. The CTE values were 8.95, 9.25, 9.22, and 9.93 × 10^{-6} $°C^{-1}$, indicating that the replacement level had a minor influence on thermal expansion.

The FA family [5], also designed for a specified compressive strength of 55 MPa, contained 0%, 10%, 20%, and 30% FA, denoted FA00, FA10, FA20, and FA30. Strengths were measured using the same specimen type, ages, and standards as those used for the SF family. The source study also reported adiabatic temperature records, hydration parameters, a fitted FA influence coefficient of 0.4 for the ultimate degree of hydration, and a coupled thermal-stress analysis of a 2.0 m × 3.0 m pier section [12]. Although the binder content and water-to-binder ratio were identical, the two programs differed in aggregate proportions, superplasticizer product (Sika ViscoCrete 151 for SF and ViscoCrete 3000-20M for FA), and initial specimen temperature (Table 1). Because the two families were produced in different experimental programs, direct absolute comparisons are supplemented by changes normalized to each family's control concrete.

Table 1. Mixture proportions of the SF and FA concretes (kg/m³) [12,13].

Mix	Cement	SF	FA	Water	Coarse aggregate	Fine aggregate	HRWR	w/b
SF00	530.0	0	0	169	1098.2	620.4	5.5	0.32
SF05	503.5	26.5	0	169	1098.2	611.8	5.5	0.32
SF10	477.0	53.0	0	169	1098.2	603.2	5.5	0.32
SF15	450.5	79.5	0	169	1098.2	594.6	5.5	0.32
FA00	530.0	0	0	170	1050.0	723.0	5.5	0.32
FA10	477.0	0	53.0	170	1050.0	709.0	5.5	0.32
FA20	424.0	0	106.0	170	1050.0	695.0	5.5	0.32
FA30	371.0	0	159.0	170	1050.0	680.0	5.5	0.32

The measurements in Table 2 reveal contrasting early tensile-strength responses to the two replacements. Relative to its control, SF increased the 1-day splitting tensile strength by 10-18% and the 2-day value by 8-15%. In contrast, FA reduced the 1-day value by 8-29%, and the 2-day value by 5-24%, and FA30 also had a 38% lower 1-day compressive strength than FA00. Because the maximum cracking indices occurred at 41-62 h (Section 4), the 2-3-day tensile strengths are directly relevant to the cracking assessment. The two control mixtures also differed: FA00 had a higher 28-day strength than SF00 but a lower 1-day splitting tensile strength (2.65 versus 3.21 MPa).

Table 2. Compressive strength f_c and splitting tensile strength $f_{ct,sp}$ of the SF and FA concretes [12,13].

Mix	f_c (MPa)			$f_{ct,sp}$ (MPa)				
	1 d	**3 d**	**28 d**	**1 d**	**2 d**	**3 d**	**7 d**	**28 d**
SF00	38.54	51.23	66.26	3.21	3.75	4.15	4.27	4.70
SF05	39.26	53.52	69.06	3.78	4.04	4.34	4.49	4.89
SF10	39.13	55.80	73.34	3.54	4.22	4.29	4.80	5.13
SF15	41.24	56.62	71.65	3.78	4.32	4.45	4.56	5.07
FA00	29.30	55.58	76.19	2.65	3.37	3.72	4.48	5.98
FA10	25.07	50.11	70.60	2.44	3.19	3.69	4.40	5.01
FA20	22.93	47.30	68.00	2.21	2.67	3.48	4.10	4.62
FA30	18.21	38.80	63.50	1.88	2.56	3.16	3.83	4.30

2.2. Adiabatic testing and ATR feature extraction

Both programs used an adiabatic calorimeter built at UTC on the concept of Lin and Chen [16]. Fresh concrete was cast in an insulated container (a 150 mm cube in the SF program), immersed in a water tank, and a heater kept the water at the measured core temperature of the specimen, ensuring negligible heat exchange with the surroundings. For the SF mixtures, hourly readings from 0 to 80 h were available. The adiabatic temperature rise at time t was calculated as $\Delta T_{ad}(t) = T(t) - T_0$, and its maximum is denoted by ATR_{max}.

To characterize the entire curve, t_{10}, t_{50}, t_{90}, and t_{95} were determined by linear interpolation at 10%, 50%, 90%, and 95% of ATR_{max}. The maximum temperature-rise rate was calculated from adjacent observations, $r_{max} = \max[(\Delta T_{ad,i+1} - \Delta T_{ad,i})/(t_{i+1} - t_i)]$. ATR at 24, 48, and 72 h describes early and late heat development. Equivalent cumulative heat was evaluated as

$Q(t) = \rho\, c_p\, \Delta T_{ad}(t)$, using mixture density and the dissertation value c_p = 1043 J/(kg·K). This is an energy equivalent under the adiabatic assumption, not a direct measurement of isothermal heat flow [17]. Because the specific heat of hydrating cementitious materials changes moderately with age [18], Q(t) should be regarded as an approximate energy indicator.

The initial concrete temperatures of SF00, SF05, SF10, and SF15 were 24.1, 29.7, 27.4, and 28.0°C, respectively. Consequently, the characteristic times and measured temperature-rise rates reflect the actual initial conditions of the tested mixtures. The fitted equivalent-age parameters were used to account for temperature effects on hydration kinetics in the subsequent structural analysis.

For the FA mixtures, the available temperature records were reprocessed using the same ATR definition, $\Delta T_{ad}(t) = T(t) - T_0$, with the initial temperature determined separately for each mixture. The FA records were logged at 0.1 h intervals up to 80 h in a calorimeter of the same design, with initial concrete temperatures of 31.1, 32.0, 31.7, and 31.3°C for FA00-FA30 [12]; the source reports only selected readings, so a complete curve-feature set comparable to Table 3 could not be extracted for the FA family. The resulting FA histories were plotted together with the SF histories over the common 0-80 h interval (Figure 1). Because the two mixture families originated from separate experimental programs, their within-family trends are emphasized when interpreting differences in heat development. The 1 h (SF) and 0.1 h (FA) intervals refer to the available records from two independent experimental programs; the different temporal resolutions are therefore explicitly retained in the present comparison. These experimental sampling intervals are distinct from the one-hour computational time step used in the EACTSA structural analysis (Section 2.4).

2.3. Hydration model and material-property development

The dissertation represented hydration by an equivalent-age formulation and a three-parameter exponential curve [4,19]. The inputs are the ultimate hydration degree α_u, the time parameter τ_u, the shape parameter β, and the apparent activation energy E_a. Ultimate heat per unit binder H_u and volumetric heat potential Q_c scale the internal source term. For FA concrete, the source study reported a fitted coefficient k_{FA} = 0.4 for the influence of FA on the ultimate degree of hydration, which is lower than the value 0.5 in the cited Schindler-Folliard formulation. These parameters link laboratory calorimetry to heat generation at non-isothermal temperatures inside the pier. Thermal conductivity was varied as $k(\alpha_r) = k_u(1.33 - 0.33\alpha_r)$, where $\alpha_r = \alpha/\alpha_u$, with k_u = 2.2 W/(m·K) [16]. Mixture densities were 2393-2419 kg/m³ for the SF family and 2436-2479 kg/m³ for the FA family, with c_p = 1042-1044 J/(kg·K) [12,13]. Compressive and splitting tensile strengths were related to the degree of hydration following De Schutter [3], using parameters fitted to the measured strengths in Table 2, and creep was represented by the B3 model calibrated according to ACI 209.2R-08 [20].

The degree of hydration was expressed as a function of equivalent age [4,19]:

$$\alpha(t_e) = \alpha_u \exp[-(\tau_u/t_e)^{\beta}] \quad (1)$$

where t_e is the equivalent age at the reference temperature T_r = 296 K, calculated from the concrete temperature history $T_c(t)$ with the Arrhenius function [4]:

$$t_e(T_r) = \Sigma\, exp[(E_a/R)(1/T_r - 1/T_c)]\, \Delta t \quad (2)$$

in which R = 8.314 J/(mol·K) and Δt is the time increment. The apparent activation energy E_a was estimated from the binder chemistry with the model of Poole et al. [21]. The rate of heat generation per unit volume of concrete is then [4]:

$$\dot{q}_h(t) = H_u\, C_c\, (\beta/t_e)(\tau_u/t_e)^{\beta}\, \alpha(t_e)\, exp[(E_a/R)(1/T_r - 1/T_c)] \quad (3)$$

where C_c is the binder content (kg/m^3), and H_u is the ultimate heat of hydration of the binder (J/kg). The theoretical volumetric heat potential $Q_c = H_u C_c$ (with consistent units) differs from $Q(t) = \rho\ c_p\ \Delta T_{ad}(t)$, which is inferred from the measured adiabatic temperature rise and represents released heat up to time t. The source-model parameters in Table 4 are retained from the original studies. Here $\dot{q}_h$ is the volumetric heat-generation rate (W/m³ when consistent SI time units are used).

2.4. Coupled temperature-stress analysis and cracking criterion

For the cross-family structural assessment, the analysis used the two-dimensional mid-height section of a 2.0 m × 3.0 m bridge pier. Temperature was calculated by finite differences and thermal stress by finite elements during the first seven days using the program EACTSA [22], which accounts for viscoelastic behaviour and the daily variation of ambient temperature. The EACTSA program was previously verified against published early-age temperature and stress responses of concrete members [22]. This earlier verification supports the computational formulation but does not constitute a separate experimental validation of the present pier-section simulations. The concrete placement temperature was 27°C, the measured ambient-temperature record was applied, and the surface convection coefficient was 13.9 W/(m²·K). The FA results were taken from [12], whereas the SF mixtures were re-analysed in the present study for the same section, model, and boundary conditions using the material inputs in Tables 2 and 4. The numerical discretization comprised a square mesh size of 5 mm, with a computational time step of 1 hour. The thermal boundary conditions included the initial concrete temperature and ambient air temperature histories.

The critical response location was the midpoint of the long side, where maximum principal tensile stress was most unfavorable. Strength and elastic modulus were updated using local equivalent age. The thermal cracking-potential index was defined as $\eta(t) = \sigma_{1,t}(t)/f_{ct,sp}(t)$, where $\sigma_{1,t}$ is the maximum principal tensile stress and $f_{ct,sp}$ is the splitting tensile strength. $\eta \geq 1.0$ indicates that modelled tensile demand reaches or exceeds available capacity; $\eta < 1.0$ is interpreted as lower modelled cracking potential. Splitting tensile strength was selected because measurements were available for all eight mixtures at several early ages using the same ASTM C496 procedure, providing a consistent experimental basis for the age-dependent tensile-capacity denominator. Hence, $\eta = 1.0$ denotes equality between the predicted tensile demand and the adopted tensile-capacity criterion, not an observed crack or a cracking probability.

The model addresses thermal stress due to hydration heat and external temperature fluctuations. The analyses do not include shrinkage or explicit reinforcement effects, so η is a comparative thermal-cracking screen rather than a probabilistic crack prediction.

Data provenance and scope of reanalysis. The FA and SF mixture proportions, measured strengths, adiabatic temperature histories, and hydration-model parameters were taken from two independent experimental programs [12,13], with additional SF strength and thermal-expansion data documented in [14]. Available temperature records were reprocessed as adiabatic temperature rise relative to the initial temperature, and SF curve descriptors were

extracted for the present comparison. The FA thermal-stress results were adopted from [12], whereas the SF thermal-stress simulations for the common 2.0 m × 3.0 m pier section were rerun with EACTSA [22]. The closely related SF-only investigation [11] is acknowledged; the contribution of the present study is the within-family normalized comparison across FA and SF.

2.5. Cross-family normalization and decision criteria

Because the FA and SF families have different control ATR values, each heat indicator X was normalized within its own family as $R_X = 100(X_0 - X_p)/X_0$. The cracking-index change was calculated as $C_\eta = 100(\eta_{max,p}/\eta_{max,0} - 1)$, where negative values are beneficial. A replacement level was judged favorable only when it reduced ATR_{max} relative to its family control, produced a negative C_η, and maintained η_{max} below 1.0. This rule prevents a low-heat but mechanically weak mixture from being designated optimal.

3. COMPARISON OF HYDRATION-HEAT CHARACTERISTICS

3.1. Silica-fume ATR curves and derived kinetic features

Each SF curve passes through an initial low-rise interval, a rapid heating period and a subsequent approach to a plateau. Increasing SF shifted the rapid-rise stage to earlier ages. The time to 50% ATR decreased from 16.88 h for SF00 to 13.59, 10.48, and 9.05 h for SF05, SF10, and SF15. Similarly, t_{90} decreased from 27.10 to 18.40 h between SF00 and SF15. Thus, SF simultaneously reduced total heat accumulation and accelerated the dominant early reaction interval.

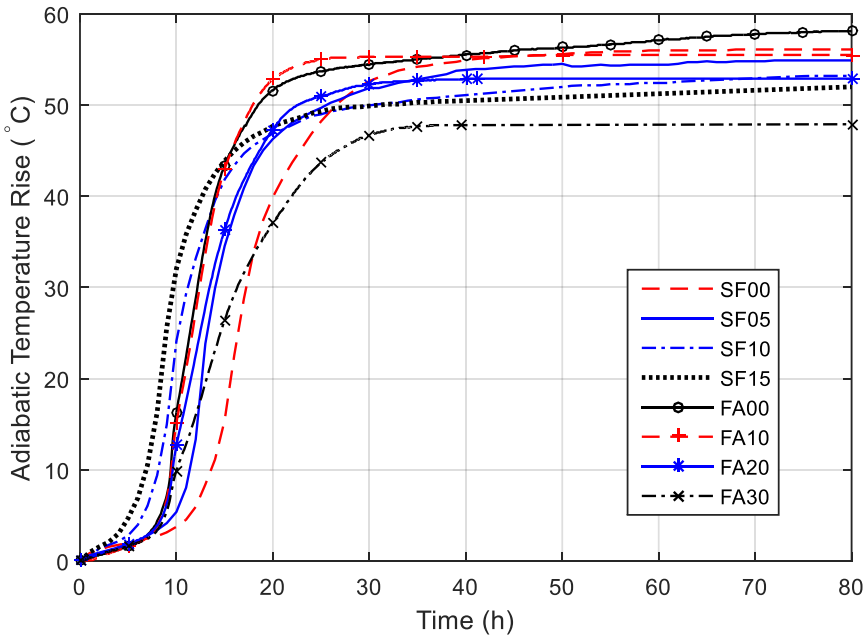


Figure 1. Experimental adiabatic temperature-rise histories of the SF and FA mixtures, replotted from the experimental datasets reported in [12,13].

Figure 1 presents the experimental adiabatic temperature-rise histories of all eight mixtures. The SF curves are first examined in this section to characterize the effects of silica fume replacement on hydration kinetics, while the comparative behavior of the SF and FA families is discussed in Section 3.3.

The maximum temperature rise rate occurred at 15.5 h for SF00, compared with 12.5, 9.5, and 8.5 h for increasing SF content. The corresponding observed rates were 7.2, 10.6, 9.1, and 9.4°C/h. These finite-difference peaks are sensitive to the one-hour sampling interval and should not be interpreted as smooth calorimetric heat-flow maxima. They nevertheless reveal that lower ATR_{max} does not imply a lower instantaneous rise rate. These rates were used to characterize the early temperature-development kinetics of the SF mixtures and were not directly incorporated into the thermal cracking-potential index η.

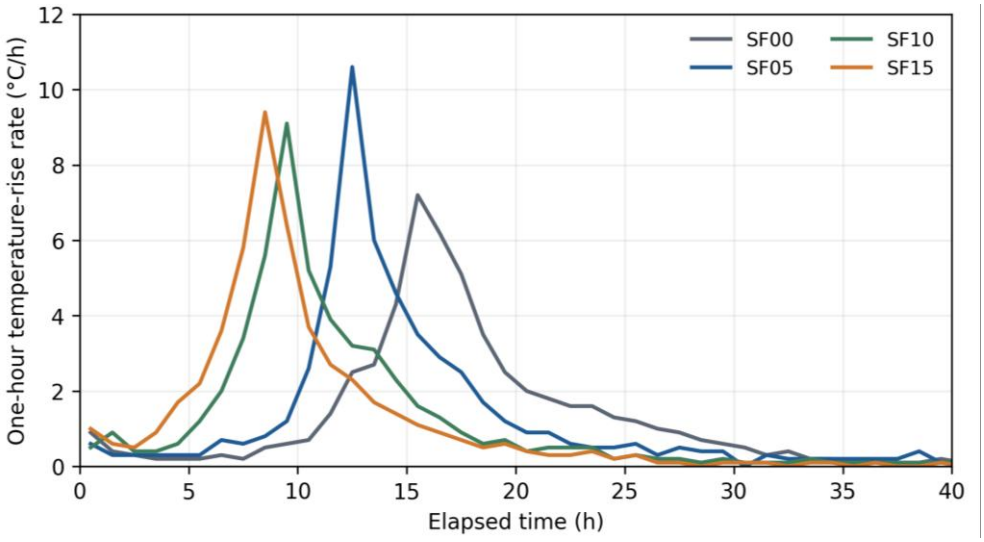


Figure 2. Temperature-rise rates derived from the tabulated SF ATR histories.

Table 3. Features extracted from the silica-fume ATR curves.

Mix	ATR_{max} (°C)	t_{10} (h)	t_{50} (h)	t_{90} (h)	t_{95} (h)	r_{max} (°C/h)	Q_{max} (MJ/m³)
SF00	56.1	11.79	16.88	27.10	31.65	7.2	141.8
SF05	54.9	10.03	13.59	24.42	31.85	10.6	138.3
SF10	53.2	6.66	10.48	22.16	34.40	9.1	133.6
SF15	52.0	5.23	9.05	18.40	25.33	9.4	130.1

The equivalent cumulative heat at the measured plateau decreased by about 8.3% from SF00 to SF15 (141.8 to 130.1 MJ/m³), which is close to the 7.3% decrease in ATR_{max}. At 24 h, however, SF10 and SF15 had already accumulated 48.8 and 49.1°C of ATR, exceeding SF00 at 46.9°C. At 48 h, ATR was 55.5, 54.4, 51.8, and 50.8°C for SF00-SF15, and at 72 h it was 56.1, 54.9, 53.0, and 51.7°C, i.e., at least 99% of the 80-h value for all mixtures. The ranking therefore depends on the time horizon: SF accelerates the early portion of the curve but lowers its eventual plateau.

3.2. Hydration-model parameters of the SF and FA mixtures

Increasing SF replacement reduced the theoretical ultimate heat H_u, volumetric heat potential Q_c, and apparent activation energy E_a, while increasing the fitted ultimate hydration degree α_u. The time parameter τ_u also decreased substantially at 10-15% SF (Table 4). These trends are consistent with two simultaneous effects: dilution of Portland cement lowers the total heat potential, whereas the fine SF particles promote dispersion and nucleation, thereby causing the rapid heat-development stage to begin earlier. The FA family showed the opposite kinetic trend: τ_u increased from 19.73 h for FA00 to 23.26 h for FA30, indicating retarded hydration,

while α_u increased from 0.610 to 0.714 and E_a decreased only slightly, from 36.0 to 33.9 kJ/mol. Thus, both admixtures lowered the total heat potential, but SF accelerated whereas FA retarded the main hydration stage.

Table 4. Hydration and thermal parameters of the SF and FA mixtures [12,13].

Mix	H_u (J/g)	Q_c (MJ/m³)	E_a (kJ/mol)	τ_u (h)	β	α_u
SF00	459.731	243.657	36.011	21.20	1.554	0.5839
SF05	436.744	231.474	33.009	20.52	1.590	0.5953
SF10	413.758	219.291	30.029	13.65	1.403	0.6037
SF15	390.771	207.109	27.071	11.56	1.561	0.6208
FA00	457.95	242.714	36.011	19.73	1.387	0.6100
FA10	414.41	219.635	35.226	20.92	1.836	0.6515
FA20	370.86	196.556	34.528	21.54	1.685	0.7027
FA30	327.32	173.478	33.916	23.26	1.567	0.7136

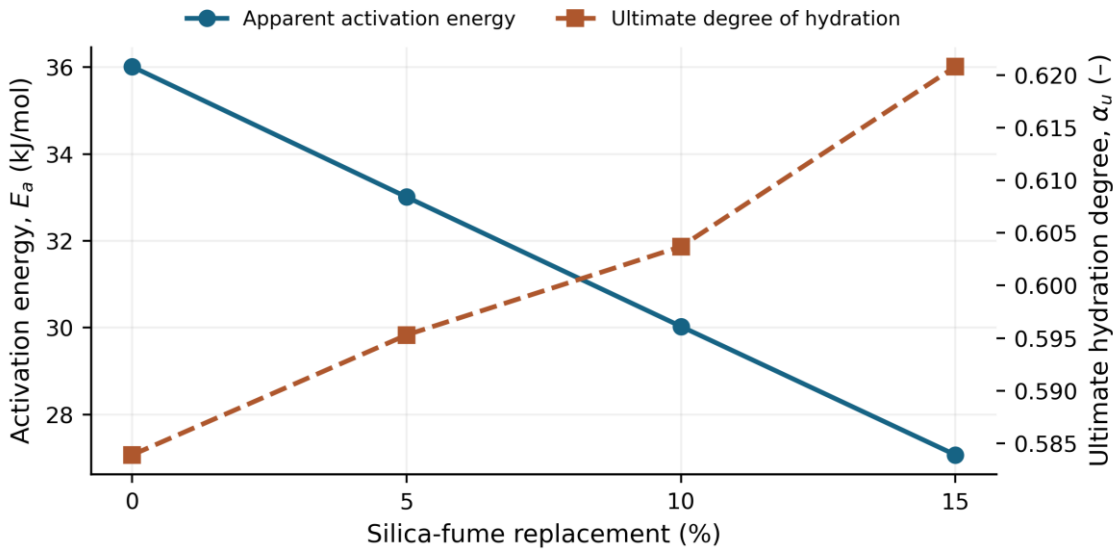


Figure 3. Effect of SF replacement on the apparent activation energy and ultimate degree of hydration.

3.3. Maximum ATR: fly ash versus silica fume

Figure 1 compares the measured ATR histories of all eight mixtures over the common 0-80 h observation period. The SF and FA curves show different patterns of early heat development; accordingly, the discussion here focuses on the maximum adiabatic temperature rise and its reduction relative to each mixture family's control. The ATR values were obtained by subtracting each mixture's recorded initial temperature from its temperature history.

The SF mixtures produced maximum ATR values of 56.1, 54.9, 53.2, and 52.0°C. Relative to SF00, the reductions were 2.1%, 5.2%, and 7.3% for SF05, SF10, and SF15. The FA mixtures produced 58.1, 55.5, 52.9, and 47.9°C, corresponding to within-family reductions of 4.5%, 9.0%, and 17.6%. The heat-release rate of the FA mixtures peaked at about 9.5 h, with peak values decreasing from 4.0×10^7 J/(h·m³) for FA00 to 2.95, 2.31, and 1.40×10^7 J/(h·m³) for FA10, FA20, and FA30 [12]. At the highest replacement level investigated, FA30 reduced ATR_{max} by more than twice as much as SF15 (Figure 4). However, the two families covered

different replacement ranges: at the common 10% level, SF10 reduced ATR_{max} slightly more than FA10 (5.2% versus 4.5%), and the reduction per percentage point of replacement was of similar magnitude for both admixtures (approximately 0.4-0.6%). The larger total reduction obtained with FA therefore reflects mainly its higher feasible replacement level.

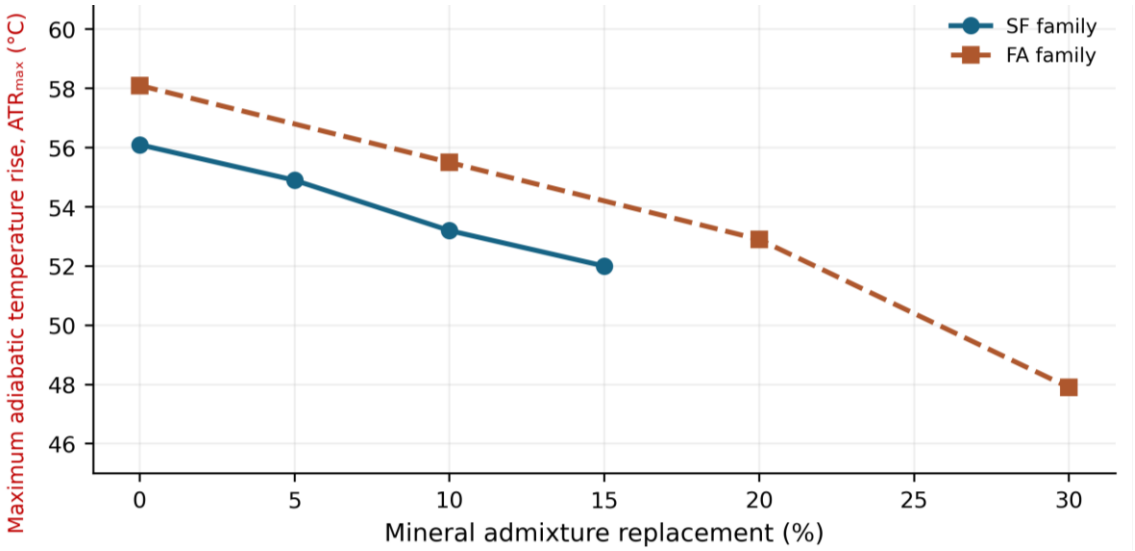


Figure 4. Maximum adiabatic temperature rise of the SF and FA mixture families [12,13].

The two unmodified controls differ by 2.0°C (58.1°C for FA00 and 56.1°C for SF00), confirming that the two families should not be treated as a single mix-design series. The more defensible comparison is the percentage change within each family. On that basis, FA provides the greater total heat reduction across the investigated replacement ranges, primarily because it is used at higher replacement levels. However, heat reduction alone does not establish cracking resistance.

4. THERMAL CRACKING POTENTIAL OF THE MASS-CONCRETE PIER

4.1. Time histories and maximum cracking index

The seven-day cracking-index trajectories in Figure 5 compare the four SF mixtures and four FA mixtures for the same 2.0 m × 3.0 m pier section over the first seven days. The horizontal line at $\eta = 1.0$ represents the adopted threshold at which the calculated maximum principal tensile stress reaches the available splitting tensile strength. Since all mixtures were evaluated using the same geometry and thermal boundary conditions, the results provide a direct comparison of their modeled thermal-cracking responses.

For the SF mixtures, η_{max} was 0.8737 for SF00, increased slightly to 0.8851 for SF05, and subsequently decreased to 0.8343 and 0.8162 for SF10 and SF15, respectively (Table 5). All four SF mixtures remained below the threshold throughout the seven-day analysis. Relative to SF00, the maximum cracking index increased by approximately 1.3% for SF05, whereas it decreased by 4.5% for SF10 and 6.6% for SF15. The results indicate that a small SF replacement did not necessarily improve the cracking index, while the 10% and 15% replacement levels produced lower maximum values under the modeled conditions.

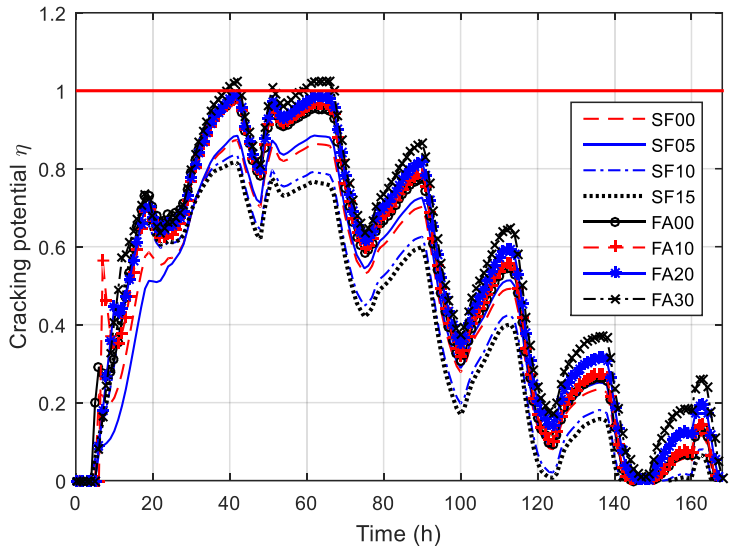


Figure 5. Time histories of the cracking-potential index (η) for the SF and FA mixtures in the 2.0 m × 3.0 m pier section. The horizontal red line indicates the threshold η = 1.0.

The FA mixtures exhibited a different response. The maximum cracking indices were 0.9793 for FA00, 0.9796 for FA10, 0.9890 for FA20, and 1.0241 for FA30. FA00, FA10, and FA20 remained below the threshold, although their maximum values were close to 1.0. In contrast, FA30 exceeded the threshold by approximately 2.4%, indicating that the calculated tensile demand exceeded the available tensile strength at the critical time. Relative to FA00, the maximum cracking index increased slightly for FA10 and FA20 and more noticeably for FA30. Thus, increasing FA replacement did not yield a corresponding improvement in the modeled cracking response, despite the greater reduction in the maximum adiabatic temperature rise. This result agrees with the source study, in which the FA30 index exceeded 1.0 between approximately 39 and 68 h [12], and with the lower early splitting tensile strength of FA30 (Table 2). It should also be noted that the two control mixtures differ markedly (η_{max} = 0.8737 for SF00 versus 0.9793 for FA00), although neither contains a mineral admixture. This difference reflects the distinct mixture proportions and tensile-strength development of the two experimental programs; cross-family comparisons of cracking potential are therefore based primarily on within-family changes (Tables 1, 2, and 6).

The peak values occurred between 41 and 62 h, depending on the mixture. The maximum cracking index occurred at 42 h for SF00, 62 h for SF05, and 41 h for both SF10 and SF15. For the FA mixtures, the corresponding times were 42 h for FA00, FA10, and FA20, and 62 h for FA30. These differences demonstrate that the critical time was mixture-dependent. As shown in Figure 5, each history contains two nearly equal peaks approximately 1 day apart (around 41-42 h and 62 h), consistent with the daily cycle of the recorded ambient temperature; small differences between mixtures determine which of these peaks governs η_{max}. The complete time histories are therefore more informative than a comparison of peak values alone, particularly for identifying the periods when the calculated tensile demand approaches or exceeds the available tensile capacity.

Interpretation of stress and strength contributions. Because η(t) combines principal tensile stress and age-dependent splitting tensile strength, the peak index alone cannot establish whether a mixture response was governed predominantly by a larger thermal stress or a smaller tensile capacity. The early-age tensile-strength values in Table 2 provide a plausible explanation

for the FA30 response, but a quantitative attribution requires the stress, temperature gradient, and tensile-strength values at the governing times (Table 5). Those outputs are not reported here and should not be inferred by back-calculation from η_{max}.

Table 5. Comparative thermal cracking indicators for the 2.0 m × 3.0 m pier (SF: present analysis; FA: [12]).

Family	Mix	Replacement (%)	η_{max}	Time of η_{max} (h)	Threshold assessment
SF	SF00	0	0.8737	42	Below 1.0
SF	SF05	5	0.8851	62	Below 1.0
SF	SF10	10	0.8343	41	Below 1.0
SF	SF15	15	0.8162	41	Below 1.0
FA	FA00	0	0.9793	42	Below 1.0
FA	FA10	10	0.9796	42	Below 1.0
FA	FA20	20	0.9890	42	Below 1.0
FA	FA30	30	1.0241	62	Above 1.0

4.2. Relationship between hydration-heat reduction and cracking potential

The two performance measures lead to different mixture rankings: a reduction in hydration heat does not necessarily lower the calculated cracking index. As shown in Section 3.3, FA produced a greater reduction in maximum adiabatic temperature rise than SF within the investigated replacement ranges. Relative to their respective control mixtures, ATRmax decreased by 17.6% for FA30 and by 7.3% for SF15. However, the cracking-index results for the common 2.0 m × 3.0 m pier section do not follow the same ranking.

Among the SF mixtures, all four had $\eta_{max} < 1.0$, with SF10 and SF15 producing the lowest maximum cracking indices. For the FA mixtures, FA00, FA10, and FA20 also remained below the threshold, although their maximum cracking indices were close to 1.0. FA30, despite providing the largest reduction in ATR_{max}, achieved $\eta_{max} = 1.0241$, exceeding the adopted threshold. To quantify the relative changes in cracking potential, the percentage change in the maximum cracking index, $C\eta$, was calculated relative to the corresponding control mixture within each family, as summarized in Table 6. Negative values indicate a reduction in the maximum cracking index, whereas positive values indicate an increase.

As shown in Table 6, SF10 and SF15 reduced η_{max} by 4.51% and 6.58%, respectively, whereas SF05 increased it by 1.31%. In contrast, FA10 and FA20 produced virtually no change in the maximum cracking index compared with FA00, whereas FA30 increased it by 4.57%. These results demonstrate that the mixture that provides the greatest reduction in maximum adiabatic temperature rise does not necessarily yield the most favorable cracking response.

Table 6. Change in η_{max} relative to family control (%)

Mix	Change in η_{max} (%)	Mix	Change in η_{max} (%)
SF00	0 %	**FA00**	0 %
SF05	1.31 %	**FA10**	0.03 %
SF10	−4.51 %	**FA20**	0.99 %
SF15	−6.58 %	**FA30**	4.57 %

This behavior is consistent with the definition of the cracking index $\eta(t) = \sigma(t)/f_{ct}(t)$, which accounts for both the calculated tensile stress and the available splitting tensile strength.

Reducing heat generation may lower thermal gradients and associated stresses, but the resulting cracking index also depends on the development of tensile strength and elastic modulus with equivalent age. Consequently, ATR_{max} alone cannot adequately represent the combined thermal and mechanical response relevant to early-age cracking.

For the investigated mixtures and the specified 2.0 m × 3.0 m pier section, SF10 and SF15 yielded the most favorable cracking-index results, whereas FA30 was the only threshold exceeder. The advantage of SF in this comparison lies in its more favorable modeled stress-to-strength ratio, rather than in achieving the largest reduction in hydration heat. These findings support the use of coupled thermal-stress analysis, rather than heat reduction alone, when evaluating mineral-admixture replacement strategies.

The assessment remains conditional on the adopted model, material properties, thermal boundary conditions, and seven-day analysis period. Values of $\eta_{max} < 1.0$ indicate that the calculated tensile demand remained below the modeled tensile capacity throughout the analysis period; they do not guarantee the absence of cracking under field conditions. Likewise, exceeding $\eta(t) = 1.0$ identifies a modeled threshold exceedance but does not independently determine the probability, width, or extent of cracks.

5. MULTI-CRITERIA ASSESSMENT AND PRACTICAL REPLACEMENT RANGE

The relative ranking of the two mixture families depends on whether the design priority is to reduce hydration heat or to improve the modeled resistance to thermal cracking. Relative to their respective control mixtures, ATRmax decreased by 2.1%, 5.2%, and 7.3% for SF05, SF10, and SF15, respectively. The corresponding reductions were 4.5%, 9.0%, and 17.6% for FA10, FA20, and FA30. Thus, FA provided greater heat reduction at the higher replacement levels investigated. However, the changes in the maximum cracking index, evaluated for the common 2.0 m × 3.0 m pier section, followed a different trend.

Table 7 summarizes the multi-criteria comparison using three indicators: the reduction in ATR_{max} relative to the control mixture within each family, the percentage change in η_{max}, and whether the maximum cracking index remained below 1.0 during the seven-day analysis. Negative changes in η_{max} indicate an improvement relative to the corresponding control mixture, whereas positive changes indicate an increase in the maximum cracking index.

Table 7. Multi-criteria comparison of the SF and FA mixtures for the 2.0 m × 3.0 m pier section.

Mix	ATR reduction (%)	Change in η_{max} (%)	$\eta_{max} < 1.0$?	Assessment
SF00	0	0	Yes	Control
SF05	2.1	1.31	Yes	Modest heat reduction; slightly higher cracking index
SF10	5.2	−4.51	Yes	Favorable balance of heat reduction and cracking response
SF15	7.3	−6.58	Yes	Most favorable combined response among the SF mixtures
FA00	0	0	Yes	Control
FA10	4.5	0.03	Yes	Heat reduction; virtually unchanged cracking index
FA20	9.0	0.99	Yes	Greater heat reduction; slightly higher cracking index
FA30	17.6	4.57	No	Largest heat reduction, but exceeds the cracking threshold

Among the investigated SF proportions, SF10 and SF15 give the most favorable combination of the selected indicators. Both reduced ATR_{max} and η_{max} relative to SF00, while maintaining the maximum cracking index below 1.0 throughout the modeled period. SF15 provided the largest heat reduction and the lowest maximum cracking index within the SF family. Nevertheless, the present results do not establish that replacement levels above 15% would yield further improvements.

The FA series exhibits a contrasting trade-off. Increasing FA replacement produced progressively greater reductions in ATR_{max}, but the maximum cracking index did not improve relative to FA00. FA10 and FA20 remained below the threshold, although their η_{max} values were close to 1.0. FA30 achieved the greatest heat reduction but reached $\eta_{max} = 1.0241$, exceeding the adopted threshold. These findings demonstrate that the effectiveness of FA in reducing hydration heat cannot, by itself, establish its suitability with respect to the modeled thermal-cracking criterion.

For the investigated 2.0 m × 3.0 m pier section, SF10-SF15 represents the most favorable combined performance within the tested SF range. This assessment considers both the reduction in hydration heat and the relative improvement in the maximum cracking index. It does not imply that every other mixture is unacceptable: SF05, FA10, and FA20 also remained below the adopted threshold, although they did not provide the same combined improvement in heat reduction and cracking response.

Study limitations. The FA and SF series were obtained from two distinct experimental programs, with differences in aggregate proportions, admixture product, and initial measurement temperatures. The within-family normalized comparisons therefore provide stronger evidence than absolute inter-family rankings. The present assessment concerns one 2.0 m × 3.0 m cross-section, the specified placement and environmental temperatures, and a seven-day thermal-stress window. The stress-to-splitting-strength ratio is a deterministic screening index, not a measured crack probability or crack-width prediction. The available cracking-index results do not permit a quantitative separation of thermal-stress and tensile-capacity contributions at the governing ages. The SF component should also be read alongside the closely related 2026 SF-only publication [11]; the distinct contribution of the present work is the normalized FA-SF comparison, not an independent claim of novelty for the original SF experimental program.

These findings should be interpreted only for the investigated high-strength concrete mixtures, the 2.0 m × 3.0 m pier section, the specified placement temperature and convection coefficient, the recorded ambient-temperature history, and the seven-day analysis period. Project-specific recommendations require the coupled thermal-stress analysis to be repeated using the actual geometry, restraint conditions, material properties, curing regime, and construction environment.

6. CONCLUSIONS

This study comparatively assessed the effects of fly ash (FA) and silica fume (SF) replacement on the hydration heat characteristics and early-age thermal cracking potential of high-strength concrete. Experimental data from two mixture series were evaluated using a consistent thermal-stress analysis of a 2.0 m × 3.0 m bridge-pier cross-section. Based on the comparative results, the following conclusions can be drawn:

- Across the two-mixture series, greater cement replacement consistently reduced the maximum adiabatic temperature rise, but the reduction differed in magnitude. Relative to their own controls, FA30 achieved a 17.6% reduction and SF15 a 7.3% reduction. At the common 10% replacement level, FA10 and SF10 produced comparable reductions of 4.5% and 5.2%, respectively.
- The standardized 2.0 m × 3.0 m cross-section revealed a different ranking when thermal cracking potential was considered. The maximum cracking index increased from 0.9793 for FA00 to 1.0241 for FA30; FA30 was the only mixture to exceed the adopted threshold of 1.0. FA10 and FA20 remained below the threshold but showed no improvement over FA00 in their maximum index.
- In the SF series, SF05 slightly increased the maximum cracking index by 1.31% compared with SF00, whereas SF10 and SF15 reduced it by 4.51% and 6.58%, respectively. Their maximum indices, 0.8343 and 0.8162, remained below 1.0 throughout the seven-day analysis.
- The contrasting trends indicate that maximum adiabatic temperature rise alone does not reliably rank the investigated mixtures by thermal cracking potential. The index also reflects the interaction of thermal tensile demand with the tensile strength developing at the corresponding age; the present data do not isolate the numerical contribution of each mechanism.
- For this cross-section, mixture dataset, and boundary-condition set, SF10-SF15 gave the most favorable joint outcome in terms of heat reduction and normalized cracking-index change. This is a conditional comparison, not a universal recommendation of SF over FA. The two source-mixture programs differed in properties beyond mineral replacement, and transferring the ranking to other members requires a renewed thermal-stress analysis.

ACKNOWLEDGEMENTS

This research is funded by University of Transport and Communications (UTC) under grant number T2025-CB-015TĐ.

REFERENCES

[1]. ACI Committee 207, ACI 207.1R-05: Guide to Mass Concrete, American Concrete Institute, Farmington Hills, MI, 2005.

[2]. ACI Committee 207, ACI 207.2R-07: Report on Thermal and Volume Change Effects on Cracking of Mass Concrete, American Concrete Institute, Farmington Hills, MI, 2007.

[3]. G. De Schutter, Fundamental study of early age concrete behaviour as a basis for durable concrete structures, Materials and Structures, 35(1) (2002) 15-21. https://doi.org/10.1007/BF02482085

[4]. A.K. Schindler, K.J. Folliard, Heat of hydration models for cementitious materials, ACI Materials Journal, 102(1) (2005) 24-33. https://doi.org/10.14359/14246

[5]. A.M. Lawrence, M. Tia, C.C. Ferraro, M. Bergin, Effect of early age strength on cracking in mass concrete containing different supplementary cementitious materials: experimental and finite-element investigation, Journal of Materials in Civil Engineering, 24(4) (2012) https://doi.org/10.1061/(ASCE)MT.1943-5533.0000389

[6]. Y. Zhang, T. Kim, A. Castel, T. Xu, Thermal cracking in high volume of fly ash and GGBFS concrete, International Journal of Concrete Structures and Materials, 17 (2023) 65. https://doi.org/10.1186/s40069-023-00626-z

[7]. M.P. Mokal, R. Mandal, S. Nayak, S.K. Panda, Impact of slag-fly ash cementitious system on thermal controls and durability of high-strength mass concrete, Structural Concrete, 24(5) (2023) 6778-6797. https://doi.org/10.1002/suco.202300197

[8]. J. Xin, Y. Liu, G. Zhang, Z. Wang, J. Wang, N. Yang, Y. Qiao, Evaluation of early-age thermal cracking resistance of high w/b, high volume fly ash (HVFA) concrete using temperature stress testing machine, Case Studies in Construction Materials, 16 (2022) e00825. https://doi.org/10.1016/j.cscm.2021.e00825

[9]. X. Li, Z. Yu, K. Chen, C. Deng, F. Yu, Investigation of temperature development and cracking control strategies of mass concrete: A field monitoring case study, Case Studies in Construction Materials, 18 (2023) e02144. https://doi.org/10.1016/j.cscm.2023.e02144

[10]. L. Li, T. Feng, Y. Li, Y. Zhang, W. Sun, Z. Liu, Evaluating the effect of high fly ash content and low curing temperature on early hydration heat of blended cement based on isothermal calorimetric method, Construction and Building Materials, 430 (2024) 136110. https://doi.org/10.1016/j.conbuildmat.2024.136110

[11]. D.T. Nguyen, T.A. Do, V.H. Hoang, T.T. Hoang, D.T. Tran, Optimized silica fume replacement for enhanced early-age thermal cracking resistance in high-performance concrete: Experimental and numerical evaluation, Frontiers of Structural and Civil Engineering, 20(4) (2026) 706-720. https://doi.org/10.1007/s11709-026-1291-y

[12]. Hoang Thi Tuyet, Study on thermal behavior and solutions for temperature control and crack mitigation in early-age high-strength concrete in bridge structures, Ph.D. dissertation, University of Transport and Communications, Hanoi, 2023 (in Vietnamese).

[13]. Tran Duc Tam, Study on the thermo-mechanical behavior of bridge structures using concrete with silica fume mineral admixture, Ph.D. dissertation, University of Transport and Communications, Hanoi, 2024 (in Vietnamese).

[14]. D.T. Nguyen, V.H. Hoang, D.T. Tran, A.T. Do, Strength development and coefficient of thermal expansion of high-strength concrete using silica fume, Transport and Communications Science Journal, 76(1) (2025) 114-123. https://doi.org/10.47869/tcsj.76.1.10

[15]. ACI Committee 211, ACI 211.4R-08: Guide for Selecting Proportions for High-Strength Concrete Using Portland Cement and Other Cementitious Materials, American Concrete Institute, Farmington Hills, MI, 2008.

[16]. Y. Lin, H.-L. Chen, Thermal analysis and adiabatic calorimetry for early-age concrete members: Part 2. Evaluation of thermally induced stresses, Journal of Thermal Analysis and Calorimetry, 124(1) (2016) 227-239. https://doi.org/10.1007/s10973-015-5131-x

[17]. ASTM International, ASTM C1679-08: Standard Practice for Measuring Hydration Kinetics of Hydraulic Cementitious Mixtures Using Isothermal Calorimetry, ASTM International, West Conshohocken, PA, 2008. https://doi.org/10.1520/C1679-08

[18]. D.P. Bentz, Transient plane source measurements of the thermal properties of hydrating cement pastes, Materials and Structures, 40(10) (2007) 1073-1080. https://doi.org/10.1617/s11527-006-9206-9

[19]. K.A. Riding, J.L. Poole, K.J. Folliard, M.C.G. Juenger, A.K. Schindler, Modeling hydration of cementitious systems, ACI Materials Journal, 109(2) (2012) 225-234. https://doi.org/10.14359/51683709

[20]. ACI Committee 209, ACI 209.2R-08: Guide for Modeling and Calculating Shrinkage and Creep in Hardened Concrete, American Concrete Institute, Farmington Hills, MI, 2008.

[21]. J.L. Poole, K.A. Riding, K.J. Folliard, M.C.G. Juenger, A.K. Schindler, Methods for calculating activation energy for Portland cement, ACI Materials Journal, 104(1) (2007) 303-311. https://doi.org/10.14359/18499

[22]. T.A. Do, H.L. Chen, G. Leon, T.H. Nguyen, A combined finite difference and finite element model for temperature and stress predictions of cast-in-place cap beam on precast columns, Construction and Building Materials, 217 (2019) 172-184. https://doi.org/10.1016/j.conbuildmat.2019.05.019